Marafão, Fernando P. and Brandão, Danilo I. and Costabeber, Alessando and Paredes, Helmo K.M. (2015) Multi-task control strategy for grid-tied inverters based on conservative power theory. IET Renewable Power Generation, 9 (2). pp. 154-165. ISSN 1752-1424

Multi-task control strategy for grid-tied inverters based on Conservative Power Theory

Dr. Fernando P. Marafão
UNESP–Univ. Estadual Paulista, SP, Brazil
Postal address: Group of Automation and Integrated Systems, Av. Três de Março 511 - Sorocaba, Brazil
fmarafao@sorocaba.unesp.br

Msc. Danilo I. Brandão
State University of Campinas, SP, Brazil
Postal address: Department of Energy System and Control, Av. Albert Eintein 400, - Campinas, Brazil
dbrandao@dsce.fee.unicamp.br

Dr. Alessandro Costabeber
University of Nottingham, NG, UK
Postal address: Department of Electrical and Electronic Engineering, NG7 2RD, Nottingham, UK
alessandro.costabeber@nottingham.ac.uk

Dr. Helmo K. M. Paredes
UNESP–Univ. Estadual Paulista, SP, Brazil
Postal address: Group of Automation and Integrated Systems, Av. Três de Março 511 - Sorocaba, Brazil
hmorales@sorocaba.unesp.br

Abstract*—In recent years, the concept of decentralizing power generation through the deployment of distributed generators (DGs) has been widely accepted and applied, driven by the growing market of renewable energy sources, in particular photovoltaic, wind and small hydro. These distributed generators are normally equipped with a switching power interface (inverter), acting as front end with the grid. In this scenario this paper proposes a multi-task control strategy for distributed generation inverters that simultaneously allows the DG system to inject the available energy, as well as to work as a voltage drop compensator or as an active power filter, mitigating load current disturbances and improving power quality of the grid. The main contribution of the proposed system, with respect to other solutions in the literature, is that the proposed control loops are based on the Conservative Power Theory decompositions. This choice provides decoupled power and current references for the inverter control, offering a very flexible, selective and powerful control strategy for the DG system. The paper also discusses the choice of the current waveform for injecting/absorbing active power into/from the grid, and both sinusoidal and resistive references have been compared in terms of damping capability. Finally, simulation and experimental results are provided in order to validate the proposed functionalities of the DG control system.

I. INTRODUCTION

Distributed generation systems (DGS) have drawn considerable attention in the last two decades, mainly for the increasing concerns about the continuous expansion of world energy demand and the consequent CO_2 emissions [1,2]. In addition to environmental support, DGSs also provide some other desirable features, such as lower infrastructure costs, energy diversification and deregulation of energy market. Moreover, some DGSs - e.g. those based on photovoltaic - can be installed close to the loads, reducing distribution losses and increasing hosting capacity with minimum infrastructure investments. Another important issue for power systems industry is power quality (PQ) control over the network, especially in presence of reactive, nonlinear and/or unbalanced loads [3-10], and DGS can be a valuable support by exploiting their inherent power control capability and flexibility. In fact, most of the DGSs are equipped with switching power interface (SPI) [11], which may be used to enhance power quality in steady state operation and/or during transient events, instead of only injecting active power into the grid [12-14]. In this context, this paper proposes a DGS control architecture capable of injecting the available energy into the grid and, simultaneously, to work as a static compensator providing voltage support at the point of common coupling (PCC) or as an active power filter (APF), mitigating the detrimental effects of distorted load currents.

This paper considers a grid-tied single-phase inverter, representing a common grid front end in residential photovoltaic installations. The same approach can be extended to three-phase systems. The reason for choosing the single-phase inverter is based on the limited complexity of its conversion system, which allows a detailed discussion of the proposed multi-task controller, as well as the fact that single-phase inverters are the most common topologies for low voltage distribution systems. The main contribution of this paper is related with the utilization of the Conservative Power Theory (CPT) [15] to propose an alternative inverter control strategy for distributed generation systems. Based on time-domain definitions, active, reactive and harmonic current injection can be performed selectively, independently of waveform distortions. As already mentioned, the tasks performed by the controller are:

1. Active power injection/absorption, to fully exploit the distributed energy resources;

2. Voltage regulation, to provide voltage support at a given PCC, by means of controlling the reactive power injection;
3. Selective compensation, to minimize load current disturbances, by means of harmonic and/or reactive current compensation.

Active power injection is based on an equivalent circuit conductance and can be set as a sinusoidal current or a resistive current, independently on the presence of grid voltage distortion. The voltage drop compensation is based on the injection of reactive current by means of a controlled equivalent reactivity. Active filtering is naturally performed by the current control of the inverter when the proper current reference has been calculated using CPT. The functionalities of the active compensator become very flexible due to the possibility of being performed selectively [16]. This feature is powerful, especially when the DGS operates close to its power/current limits, where the prioritization of specific electrical disturbance compensation becomes relevant and useful.

Beyond its flexibility and selectivity, the proposed method differs from others existing solutions for the fact that it doesn’t need any kind of reference-frame transformation (as [5] and [6]); discrete Fourier transformer (as [7]); Instantaneous Power Theory (as [8]) or synchronization algorithm (as [9] and conventional harmonic current compensation), which might show nontrivial power control errors, slow dynamic response, DC real and reactive power bias or inaccuracy under distorted voltages. The proposed method does not need a synchronization algorithm, and therefore its dynamic response and steady state performance are related only with the designed voltage and current controllers.

Even if recent controllers overcome most of the limitations suffered in the past, it is also worth to mention that the computation complexity of the proposed method is limited to the discrete implementation of the controller and to two divisions needed to calculate the CPT equivalent conductance and reactivity. As shown in section VI, the control strategy has been implemented in a fixed-point digital signal processor (DSP), without encountering particular issues.

II. Conservative Power Theory – Brief Review for Single-Phase Systems

The Conservative Power Theory, proposed by Tenti et al. in [15], is defined in time domain for general (sinusoidal or non-sinusoidal) operating conditions, and can be applied to single-phase and poly-phase systems, with or without neutral conductor. The CPT proposes an orthogonal decomposition of current and power in the stationary (*abc*) frame, according to terms which are directly related to the load electrical characteristics, such as: average power transfer, reactive energy, nonlinearities and unbalances.

Assuming a single-phase circuit under periodic operation, where v, i and $\hat{v}$ are, respectively, the instantaneous values of voltage, current and the unbiased voltage integral - i.e. the AC component of the voltage integral-, the CPT defines the instantaneous active power (p) and the instantaneous reactive energy (w) and their average values as:

$$P = \overline{p} = \langle v, i \rangle = \frac{1}{T}\int_0^T v(t).i(t)dt \;\; ; \qquad W = \overline{w} = \langle \hat{v}, i \rangle = \frac{1}{T}\int_0^T \hat{v}(t).i(t)dt \; . \tag{1}$$

Such quantities are conservative in every electrical network, independently on current and voltage waveforms. The only requirement is a steady-state periodic operation. Moreover, by using the CPT, the PCC instantaneous total current can be decomposed into active current (i_a), non-active current (i_{na}), reactive current (i_r) and void current (i_v), as following:

$$i = i_a + i_{na} = i_a + i_r + i_v \; . \tag{2}$$

The active current has been defined as:

$$i_a = \frac{P}{\|v\|^2}.v = G.v \; , \tag{3}$$

where G represents the load equivalent conductance and $\|v\|$ means the voltage Euclidian norm or RMS value. The non-active current (i_{na}) is the remaining part of the total current and it is calculated by the difference:

$$i_{na} = i - i_a \; . \tag{4}$$

The reactive current has been defined as:

$$i_r = \frac{W}{\|\hat{v}\|^2} . \hat{v} = B . \hat{v} \ , \qquad (5)$$

where B represents the load equivalent reactivity and $\|\hat{v}\|$ is RMS value of the unbiased voltage integral. The void current is the residual term, which depends on the voltage and the current distortion (harmonics):

$$i_v = i_{na} - i_r = i - i_a - i_r \ . \qquad (6)$$

This current does not convey active power nor reactive energy, and reflects the presence of harmonic scattering and current harmonics generated by the load [15,17].

By definition, all the terms are orthogonal (decoupled) to each other. Then:

$$\|i\|^2 = \|i_a\|^2 + \|i_r\|^2 + \|i_v\|^2 \ . \qquad (7)$$

Thus, the apparent power may be calculated as:

$$A^2 = \|v\|^2 . \|i\|^2 = P^2 + Q^2 + D^2 \ . \qquad (8)$$

The active power (P) is related to the average power transfer. The reactive power (Q) is related to the reactive energy and the void power (D) is related to the current and voltage distortions (nonlinearities). Unlike the active power and reactive energy, the apparent, reactive and void powers are non-conservative quantities [15].

Finally, the power factor is calculated as following:

$$\lambda = \frac{P}{A} \ . \qquad (9)$$

The previous definitions can be extended to three-phase circuits as shown in [15]. Note that all the equations are valid independently on the grid voltage waveform, which could also be distorted or unbalanced (three-phase case).

III. PROPOSED MULTI-TASK CONTROLLER

The proposed multi-task controller is capable to: 1) generate sinusoidal or resistive active current injection/absorption; 2) provide voltage support managing reactive power and 3) selective reactive and void current compensation.

Fig. 1 indicates the block diagram of a generic distributed single-phase generation system including the power circuit and its control scheme. The left side block (RES) represents any sort of renewable energy source (RES), including a DC-DC first stage if required. This paper focuses on the DC-AC inverter control strategy, which is based on three main control loops required to perform the inverter functionalities.

The *output current control loop* is responsible for injecting the desired inverter current (i_{inv}^{*}) at the PCC. The *DC link control loop* regulates the DC link voltage. The *DC current control loop* guarantees that the inverter output current does not present any DC component (M_A means moving average filter). These last two control loops are decoupled from the first one assuming a design that ensures adequate difference between the respective crossover frequencies.

Note that in Fig. 1 there is a *supervisory control* block, an additional degree of freedom enabling the definition of the voltage waveform used in the *current decomposition* by the *CPT* block, *DC link control loop* (v'^{*}) and *active current reference* (v''^{*}). These voltage signals can correspond either to the measured PCC voltage (v_{PCC}) or to its fundamental component (v_{PCC}^{f}). In the following sub-sections, the main parts of the control scheme in Fig.1 will be described to highlight their role in the proposed multi-task control approach.

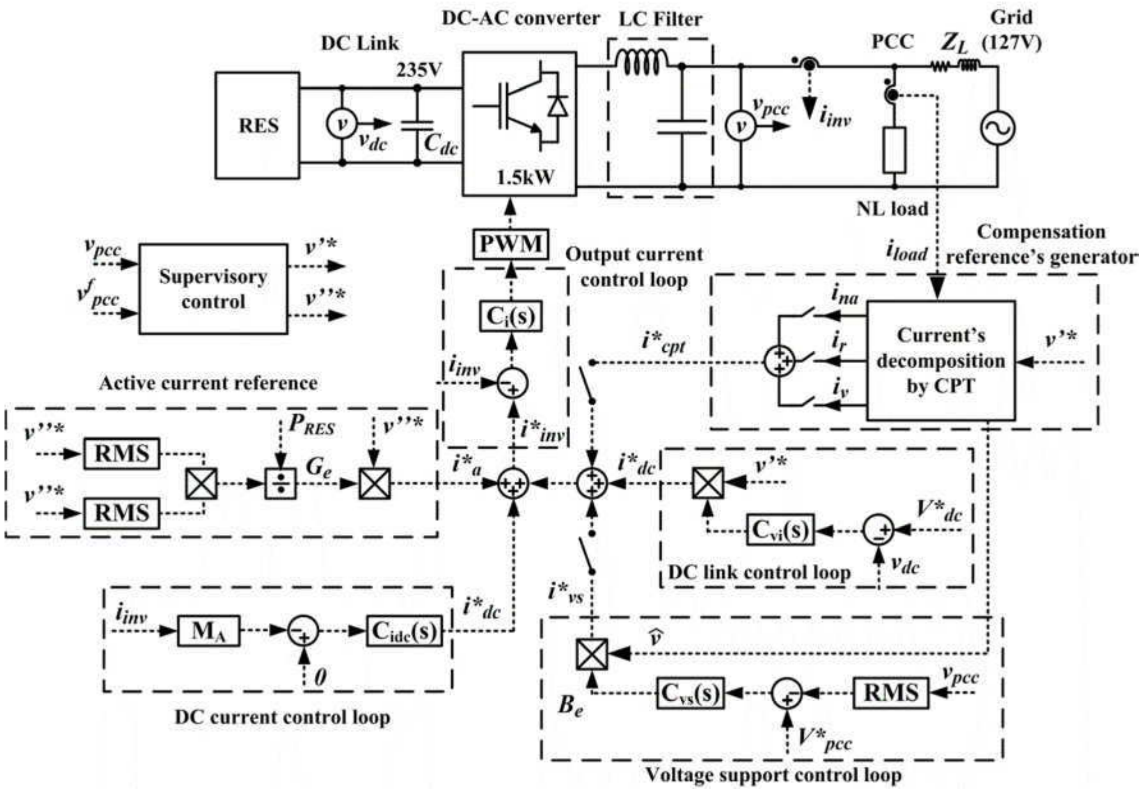

Fig. 1. Block diagram of the proposed distributed generation system.

A. Active current reference generation

From the scheme in Fig. 1, the controllable active current reference to be injected/absorbed (i_a^*) comes from the equivalence conductance (G_e), which is based on the PCC voltage and on the available power (P_{RES}) to be transferred from the RES to the AC grid. The waveform of this current reference can be calculated either from the measured PCC voltage (v_{PCC}) or from its fundamental component (v_{PCC}^f), leading to resistive (RCI) or sinusoidal (SCI) current injection, respectively. Under certain conditions and from the power quality point of view, the results of these two injection strategies may be significantly different, as discussed later in section IV and V.

Note that (i_a^*) refers to the controllable component of the active current, added to the active current component coming from the *DC link control loop* (i_{dc}^*), that guarantees the DC voltage regulation through power balance between RES and grid. Also for (i_{dc}^*), the current waveform absorbed from the grid can be either resistive (RCA) or sinusoidal (SCA), depending on the voltage reference. Note that the signal of P_{RES} defines the direction of the active power flow. It must be observed that the DC link control loop is normally enough to guarantee the power balance between the RES and the grid, but when the information on P_{RES} is available from the source, the generation of the additive term (i_a^*) acts as a feed-forward control term improving the dynamics of the DC link voltage regulation.

B. Compensation reference generator

As previously mentioned, the CPT can provide the current reference (i_{CPT}^*) to compensate, selectively or not, the load current disturbances [16]. So, each decomposed current term (i_{na}, i_r and i_v) can define a different compensation strategy, which can be included on the DGS in order to maximize its utilization and improve the power quality at the PCC. Of course, the DGS compensation functionality should be activated only when the system is not using the full inverter capability to inject active power into the grid or in case of other financial or technical constraints [3].

Moreover, since the main CPT current decompositions (active and reactive currents) are based on the concepts of proportionality and orthogonality with respect to a certain voltage reference, such voltage choice is crucial. Thus, if the PCC measured voltage is directly used for the CPT decompositions, after compensating the non-active load current the equivalent system (loads plus DG) is seen by the grid as an equivalent resistive load, absorbing a current proportional to the instantaneous grid voltage waveform, including all the harmonics. On the other hand, if the voltage fundamental component is used for the CPT decompositions, the result after the compensation is a pure sinusoidal current, in phase with the fundamental voltage. These two active compensation approaches are known as resistive load synthesis (RLS) and sinusoidal source current synthesis (SSC) and under certain circumstances, they might lead to quite different results [18,19]. It is important to highlight that both the RLS and SSC compensation approaches are based on the CPT current decomposition.

Sections V and VI will compare and discuss the results when RLS or SSC injection strategy is adopted by the DG control system.

C. Voltage support reference

The *voltage support control loop* injects reactive current (i_{vs}^{*}) at the PCC to keep the voltage within a predefined profile. The concept of voltage regulation through reactive power injection using distributed inverters was first proposed in [20], where a droop function was also included to prevent interactions between multiple inverters acting on the same feeder. In the multi-task controller, the output of the voltage support controller [$C_{vs}(s)$] corresponds to an equivalent reactivity (B_e), which is needed to retain the PCC voltage within the desired level. Depending on the sign of the controller output, the resulting reactive current reference (i_{vs}^{*}) can either increase or decrease the PCC voltage level, allowing dynamic voltage regulation [21].

However, similarly to the harmonic currents compensation, the voltage support functionality can be activated only when the DG is not injecting its nominal power into the grid or in case of particular financial or technical constraints.

It must be pointed out that the dynamic voltage support performed by injecting reactive power with the DG requires the additional hypothesis of operating the DG in a grid with inductive cables. Instead, if the cables are mainly resistive, the injection/absorption of more reactive power than the amount needed to feed the reactive demand of the local load would mainly result in additional losses, instead of in voltage variations. In this sense, the proposed solution is more suitable for three-phase converters connected to medium voltage systems, where the hypothesis is verified.

D. Further considerations about the mult-task control scheme

Except for the *output current control loop* [$C_i(s)$], all the controllers in Fig.1 are based on PI regulators, designed with classical methods, such as frequency response analysis [22]. Table I reports the basic parameters and the corresponding controllers information, where f_C and *PM* are the designed crossover frequency and phase margin. Instead, for the *output current control loop*, a proportional plus resonant controller has been applied and designed as discussed in [23]. All odd harmonics from the fundamental to the eleventh order have been included as resonant terms.

It is important to highlight that the proposed multi-task control may be equally applied for different power and voltage rating or in a three-phase system, simply changing the design of the passive and active devices and the controller gains. It is also independent on the specific RES.

TABLE I. SYSTEM AND CONTROLLERS SPECIFICATIONS.

DC-AC converter			
P=1.5kVA; V_{ac}=127V; V_{dc}=235V; L_f=1.5mH; R_f=0.056Ω; C_f=2μF.			
$C_i(s)$	$C_{vi}(s)$	$C_{vs}(s)$	$C_{idc}(s)$
f_c=1kHz; *PM*=60°.	f_c=1Hz; *PM*=50°.	f_c=5Hz; *PM*=75°.	f_c=20Hz; *PM*=75°.

IV. ANALYSIS OF THE DISTRIBUTED GENERATOR ON DAMPING HARMONIC RESONANCES

This section attempts to investigate the influence of the distributed generator (DG) on the system frequency response, when the inverter is controlled to inject or absorb active power and at the same time acts as an active power filter. Fig. 2.a and Table II show the proposed circuit and related parameters chosen for the analysis.

In addition to a local nonlinear load (*NL Load*) and a distributed generator, the proposed circuit considers an inductive-resistive (RL) load connected to node N_1. The capacitor bank (C_b) is designed to compensate the *RL load* reactive power. However, the capacitor bank and the line impedance (Z_1) produce a resonance frequency close to the eleventh harmonic of the line frequency. Besides, the non-ideal grid source is set to have 1% of eleventh harmonic, leading to an accentuated voltage distortion at the PCC. The DGS structure is the same reported in Fig. 1.

In an equivalent representation, DGS can be considered as an ideal controllable current source, in parallel with its output capacitor. The *NL load* is connected in parallel and it can be represented by a harmonic current source. This simplified modelling strategy turns the circuit of Fig. 2.a into the one shown in Fig. 2.b. Besides, applying the superposition principle under the assumption of linear circuit and independent source models, the two circuits in Fig. 2.c and Fig. 2.d can be derived [24]. Fig. 2.c assumes that the load harmonic current source is an open circuit, whereas Fig. 2.d assumes the voltage source as a short circuited. Z_3 is the equivalent impedance including Z_{RL} and Z_{cb}.

TABLE II. SIMULATION AND EXPERIMENTAL SETUP PARAMETERS.

Grid	*ResC*	*DGS*	*NL load*
127V (60Hz)	Z_{RL}=17+j4Ω Z_{Cb}=0.2-j74Ω Z_1=0.06+j0.56Ω Z_2=0+j0.06Ω	Z_f=0.06+j0.56Ω Z_{Cf}=0.05-j1300Ω R_{RES}=54Ω	L_{ac}=5mH C_{dc}=2.3mF R_{dc}=15Ω R_{ac}=48Ω

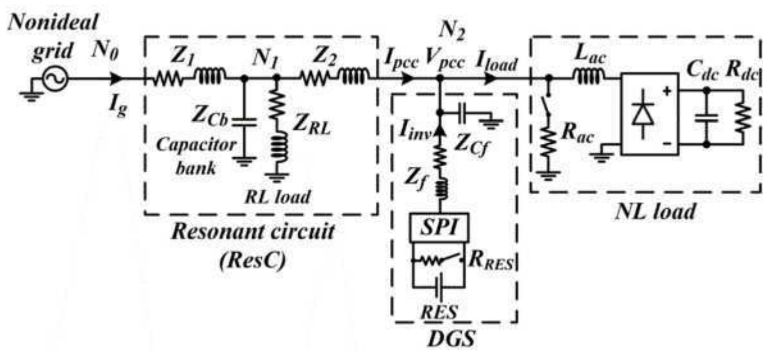

(a) Simulation and experimental circuit configuration.

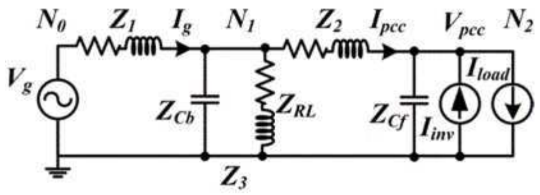

(b) Equivalent circuit of the circuit configuration.

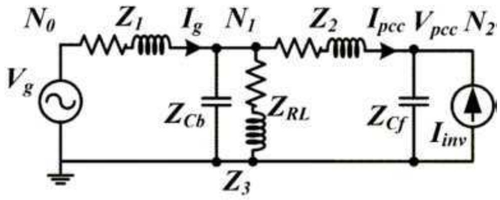

(c) equivalent circuit without load harmonic current.

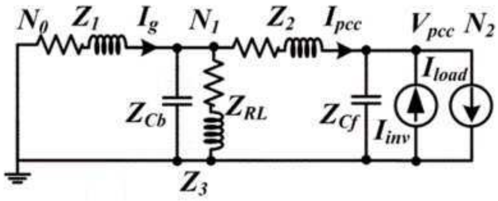

(d) equivalent circuit without voltage source.

Fig. 2. Circuits and equivalent circuits from superposition analysis of the simulation and experimental circuit.

A. Active power absorption

In order to analyze the effect of the DGS when absorbing power from the grid, we consider the circuit of Fig. 2.c. Let us assume that the voltage source (V_g) is sinusoidal. Then, the ideal controlled current (I_{inv}) is represented by (10) for a sinusoidal active power absorption (SCA) or by (11) for a PCC voltage waveform active power absorption (RCA) [25].

$$I_{inv} = k.V_g \ , \tag{10}$$

$$I_{inv} = k.V_{pcc} \ . \tag{11}$$

Observe that k=0 means that the DGS is disconnected.

From (11), corresponding to RCA, the ratio between the PCC voltage and the distributed generator current can be easily found in the frequency domain as:

$$\frac{V_{pcc}(s)}{I_{inv}(s)} = \frac{1}{k} \ , \tag{12}$$

which means that the DGS operates as a resistor. Note that the k is the equivalent conductance.

Similarly, the relation between the PCC voltage and the inverter current for sinusoidal active power absorption (SCA) is:

$$\frac{V_{pcc}(s)}{I_{inv}(s)} = \frac{Z_3(s).Z_{cf}(s)}{k.[Z_1(s)+Z_3(s)].[Z_2(s)+Z_{cf}(s)]} + \frac{[Z_1(s)//Z_3(s)+Z_2(s)].Z_{cf}(s)}{[Z_1(s)//Z_3(s)+Z_2(s)]+Z_{cf}(s)} \ , \tag{13}$$

which represents the effect of the DGS absorbing active current with fundamental waveform.

To compare SCA and RCA strategies, the bode diagrams of (12) and (13) are shown in Fig. 3.a. As expected, the RCA presents a constant behavior (true within the limits of the current control bandwidth), whereas the SCA presents a resonant peak around 690Hz, which can accentuate the harmonic components close to this frequency. The plots have been drawn considering k=0.05, which means an active power of 800W (127V) absorbed by the DGS.

Then, assuming that the resistive current absorption (RCA) is the most appropriate strategy to absorb power from the grid, the analysis of the damping effect caused by DGS can be realized by means of the input impedance observed from the grid. To this purpose, the DGS has been replaced with a conductance equal to k. The grid input impedance is shown in (14) and its bode diagram is reported in Fig. 3.b. Note that the damping increases when the DGS is absorbing active power. It has the same effect as a resistor in the end of the feeder [26].

$$\frac{V_g(s)}{I_g(s)} = Z_1(s) + \frac{\left[Z_2(s) + Z_{cf}(s) // {}^{1}/_{k}\right] . Z_3(s)}{\left[Z_2(s) + Z_{cf}(s) // {}^{1}/_{k}\right] + Z_3(s)} \ . \qquad (14)$$

B. Active power injection

Now, in order to analyze the influence of the DGS when injecting power into the grid, the circuit of Fig. 2.d is considered. The corresponding input impedance seen from the PCC is given by:

$$Z_{pcc}(s) = \frac{V_{pcc}(s)}{I_{pcc}(s)} = Z_2(s) + \frac{Z_1(s) . Z_3(s)}{Z_1(s) + Z_3(s)} \ . \qquad (15)$$

The bode diagram of (15) is shown in Fig. 3.c. It indicates that when the DGS injects active power and the active current flows to the grid through Z_{pcc}, the voltage drop on Z_{pcc} affects the grid side. This effect is amplified for the frequencies where the magnitude of Z_{pcc} increases. So, according to Fig. 3.c, the current harmonic components between 100Hz and 2kHz and higher than 3kHz will be accentuated, causing a raise in the PCC voltage THD.

It means that injecting active power with sinusoidal 60Hz waveform (SCI) is better than injecting a current proportional to the voltage waveform (RCI), since this might amplify harmonics within the specific frequency range.

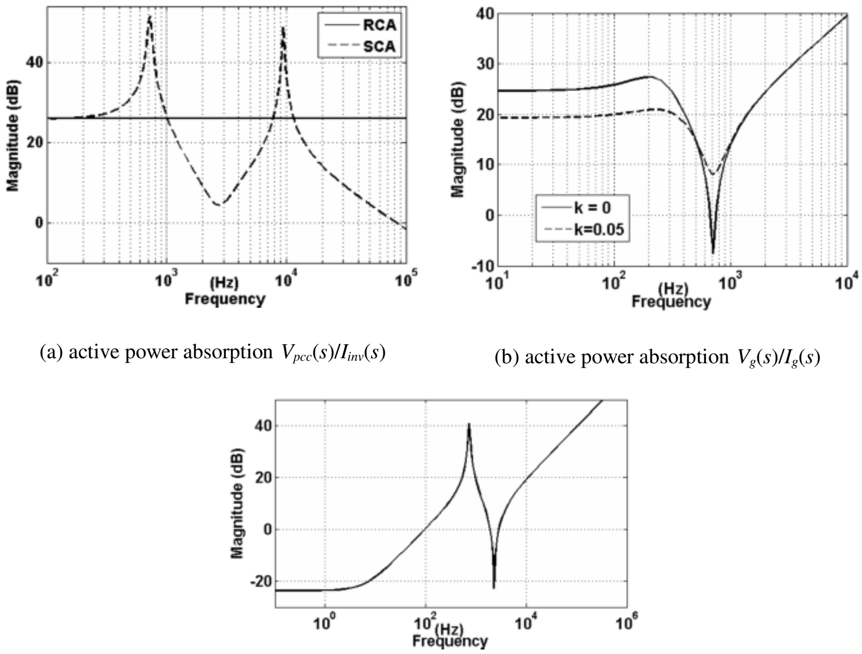

(a) active power absorption $V_{pcc}(s)/I_{inv}(s)$

(b) active power absorption $V_g(s)/I_g(s)$

(c) PCC impedance for active power injection.

Fig. 3. Bode diagram of the analysis of the distributed generator on damping harmonic resonances.

C. Load current compensation

The load current compensation (active filtering mode) analysis is very similar to the active power absorption. The main difference is that we can use the circuit of Fig. 2.b and we analyze the PCC current (I_{pcc}) rather than the inverter current (I_{inv}).

The transfer functions and bode diagrams are the same, as well as the conclusions. So, the compensation function based on the resistive load synthesis (RLS) is considered better than the sinusoidal source current synthesis (SSC), since the resulting compensated system (loads and DGS) will be seen as an equivalent resistor [19].

V. Simulation results

In order to provide a first validation of some of the proposed functionalities of the DGS, as well as the approximated analysis proposed in section IV, the circuit shown in Fig. 2.a has been implemented in PSIM software. The simulation and experimental setup parameters are reported in Table II.

A. Resistive current versus sinusoidal current references for active power injection and disturbances compensation

Considering the expectations deriving from the approximated modelling proposed in section IV, this sub-section investigates the behavior of the DGS operated either injecting or absorbing active power and compensating load current disturbances by referring to the PCC voltage or to its fundamental component.

The resonance in the circuit of Fig. 2.a is a very critical and interesting case to evaluate the behavior of the DGS and the resulting PCC voltage distortion, according to the different voltage references adopted for the CPT decomposition. For the active current, the following cases were considered: resistive current injection (RCI) and absorption (RCA) and sinusoidal current injection (SCI) and absorption (SCA). For the RCI and SCI cases, the resistor R_{RES} has not been connected to the DC link, whereas for the RCA and SCA cases it has been connected, making the inverter to operate as a controlled rectifier.

Concerning to the load current compensation strategy (active filtering mode), the following cases have been analyzed: resistive load synthesis (RLS) and sinusoidal source current synthesis (SSC). The load current compensation is first tested with zero active power exchange, and then it is validated in case on which the DGS injects about 800W of active power.

Table III summarizes the main results for the different control combinations. Although the details of the experimental setup will be presented in section VI, both simulation and experimental results are included in Table III, to anticipate the comparison. "Trip" means that experimental system protections were triggered due to high value of voltage and/or current caused by resonance.

As expected from section IV-C, when the DGS works as an active filter, without managing active power, the RLS strategy has shown to be the best choice, because it increases the damping capacity against induced resonances.

It is also possible to conclude that independently on the load current compensation strategy, the active power injection based on sinusoidal current reference (SCI) is always better, because it results in lower voltage THD (see Fig. 3.c). Instead, it is more convenient to absorb active power with resistive current reference (RCA), because it increases the damping effect at the PCC, as shown in Figs. 3.a and 3.b.

TABLE III. ACTIVE POWER INJECTION/ABSORPTION ANALYSIS.

Compensation	**Active**	**PCC voltage**	**PCC voltage**

strategy	current strategy	THD (simulation)	THD (experimental)
---	---	8.83%	9.42%
SSC	---	3.34%	3.68%
RLS	---	1.80%	2.56%
---	SCI	9.78%	9.10%
	RCI	28.58%	Trip
---	SCA	9.96%	8.68%
	RCA	7.98%	7.94%
SSC	SCI	3.64%	3.35%
	RCI	68.50%	Trip
RLS	**SCI**	1.75%	2.10%
	RCI	2.44%	2.89%
SSC	SCA	3.66%	4.15%
	RCA	2.04%	2.88%
RLS	SCA	1.80%	2.70%
	RCA	1.48%	2.15%

These results confirm that depending on the active power flow direction, the supervisory control should select the most appropriate operation mode (Table III).

B. DGS voltage support functionality

In order to validate the voltage support function, the *capacitor bank*, *RL load* and Z_2 impedance have been disconnected from the circuit of Fig. 2.a, resulting in the simplified circuit shown in Fig. 4.a, with a voltage drop of about 6% over the line impedance (Z_1). Note also from Table II that the resulting total line impedance has a reactance to resistance ratio of ten, confirming the inductive nature of the connection. This extreme condition emulates a weak power grid. The RES considered here is a photovoltaic modular string with a boost DC-DC converter.

From Fig. 4.b, before activating the voltage support function, the PCC voltage is 119V. After activating the voltage support (0.55s), the PCC voltage is increased to 125V, which corresponds to the predefined reference value (V_{PCC}^{*}). The controller output C_{vs} represents the equivalent reactivity needed to boost the voltage. However, the voltage support is possible only if the SPI is not using its full capacity to inject active power to the grid. When the available energy increases on the RES side (0.96s), the voltage support function must be inhibited in order to respect the converter limits without reducing the active power injection. It can be observed that the resulting PCC voltage is slightly higher than the initial value, since the voltage drop is decreased by means of the bigger RES active power injection.

Note that the spike in the DC power is a consequence of the dynamics of the chosen maximum power point tracking (MPPT) technique in response to an irradiation step. The simulation result has been generated using Beta MPPT technique [27].

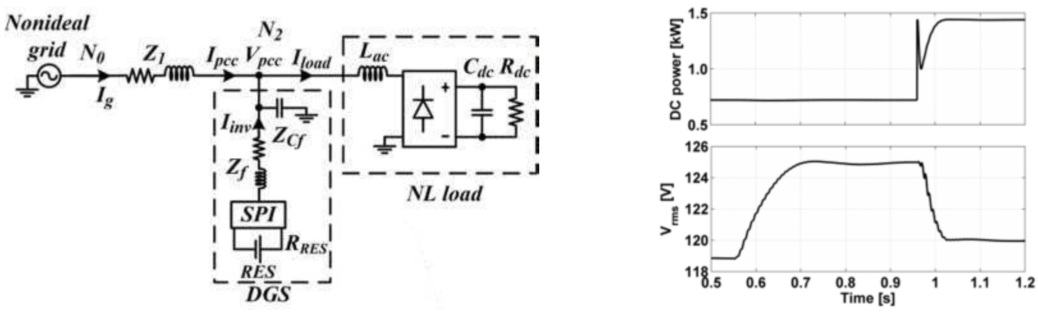

(a) analyzed circuit. (b) simulation result.

Fig. 4. Analyzed circuit and simulation result for the voltage support functionality.

C. DGS selective compensation capability

Five different conditions have been simulated in order to validate the selective compensation capability of the proposed controller. For these results the R_{RES} has been disconnected from the circuit in Fig. 2.a and an additional load R_{ac} has been connected to the circuit to increase the active power demand, as shown in Fig. 5. Fig. 6 and Table IV shows the results for the DGS operating as a selective active power filter, by means of the proposed CPT current decompositions.

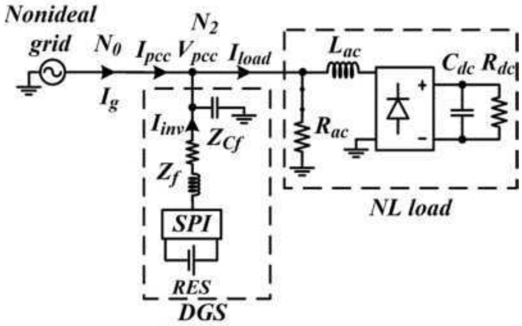

Fig. 5. Circuit for analyzing the selective compensation capability.

Non-Compensation (*NC*) means that the DGS is only injecting active power (about 600W). The inverter current is based on sinusoidal injection, since from previous discussions it was concluded to be the best option for injecting active power (SCI). In each of the other compensation conditions (i_{na}, i_r and i_v), besides the active power injection (i_a^*, i_{idc}^*), the DGS runs as active compensator, using different current reference (i_{CPT}^*).

In the last interval the system operates under 30% of voltage sag at the grid side for about five cycles, showing the ride-through capability of the proposed control. Note that the grid voltage is quite distorted during all the simulation, with a THD at the PCC equal to 6.6%, which doesn't affect the proposed control scheme.

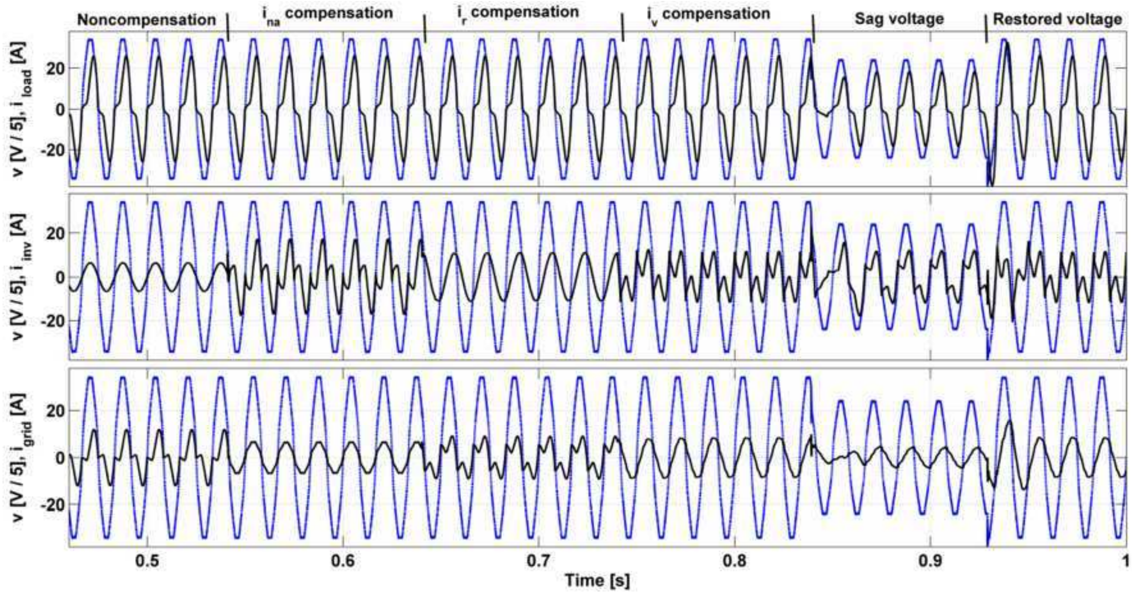

Fig. 6. Simulation result of the DGS acting as a selective compensator: PCC voltage (dashed); load, inverter and grid currents.

TABLE IV. CPT POWER TERMS, VOLTAGE AND CURRENTS ACCORDING TO DIFFERENT CONTROL STRATEGIES.

	Load	***NC (i_a)***	***i_{na}***	***i_r***	***i_v***
A [kVA]	1.92	1.48	1.08	1.25	1.34
P [kW]	1.62	1.05	1.08	1.08	1.05
Q [kVAr]	0.82	0.83	0.00	0.00	0.83
D [kVA]	0.61	0.62	0.05	0.62	0.05
λ	0.844	0.710	1.00	0.864	0.783
V_{pcc} [V]	126.98	127.02	127.19	127.18	126.99
THD [%]	6.92	6.98	6.65	6.98	6.63
I_{grid} [A]	15.01	11.46	8.36	9.69	10.40
THD [%]	33.33	45.86	7.03	58.84	7.10

I_{inv} [A]	---	4.65	9.19	7.81	6.67
THD [%]		2.42	60.4	2.30	103.60

Observe that in the non-active current (i_{na}) compensation the grid current assumes the same waveform of the PCC voltage, being the RLS the best compensation strategy.

In Table IV, except for the "*Load*" column, all the power values refer to the PCC. Note that the difference between the load active power and the PCC active power corresponds to the power from the RES (about 600W). Moreover, since the CPT current components are completely decoupled (orthogonal), depending on the choice of the current reference, each power quality disturbing effect can be selectively compensated, as indicated by the power components in Table IV. Note that injecting active power into the grid decreases the global power factor (λ), because from the PCC point of view only the active power is reduced, whereas the reactive and void powers remain the same. This highlights the importance of the load current compensation performed by the DGS.

From the columns *NC* (i_a) and i_r, where the i_{inv} is sinusoidal (SCI), it is possible to verify the steady state performance of the output current controller [$C_i(s)$] and the effectiveness of the output LC filter by means of the inverter current THD, which is 2.4%.

VI. EXPERIMENTAL RESULTS

The experimental setup is based on the control scheme and circuits of Fig. 1 and Fig. 2.a (refer to Table II for the values of the impedances). The DC-AC conversion stage is a full bridge inverter, with IGBT modules (SKM 75GB128D, driven by SKHI 23/12 – both from Semikron). The voltage and current Hall-effect sensors are from LEM and the control board is a Texas Instruments TMS320F2812. The sampling and switching frequency is set 12 kHz. The *NL load* is an uncontrolled rectifier with capacitive filter, representing a usual example of nonlinear load in low voltage distribution systems [28]. A picture of the experimental set-up is shown in Fig. 7.

(a) front view (b) back view

Fig. 7. Picture of the experimental prototype.

A. Resistive current versus sinusoidal current for active power injection and current disturbances compensation

This section investigates the experimental results anticipated in Table III (in section V-A) regarding to the management of the active power.

Fig. 8 shows the grid {4} and PCC {3} voltages, as well as the currents through Z_1 {1} and Z_2 {2} line impedances, without the DGS. It is possible to observe that the PCC voltage is quite distorted by the combined effect of the nonlinear load and the resonance, since the grid voltage has 0.4% of the eleventh harmonic order. Table V shows the grid and PCC voltages harmonic spectra, whereas the RMS values and THDs for the grid and PCC voltages are, respectively: 119.3V (3.3%) and 116.6V (9.42%).

In order to analyze the DGS damping capability against induced resonances, three conditions are tested in Fig. 9 (a-f) and discussed by means of the resulting PCC voltage and Z_2 current (refer to table III for the exact measurements).

Figs. 9.a and 9.b show the DGS running as an APF with SSC and RLS compensation strategies, respectively. As emphasized in section IV-C, the RLS provides more damping effect than the SSC compensation.

Figs. 9.c and 9.d show the DGS compensating the load current disturbance by RLS strategy and at the same time injecting about 800W of active power into the grid by SCI (Fig. 9.c) and RCI (Fig. 9.d). The PCC voltage in Fig. 9.c (SCI) is slightly less distorted than the Fig. 9.d (RCI). Z_2 current is very small due to the DGS is compensating all the load current disturbances and providing the main portion of the active power to the load.

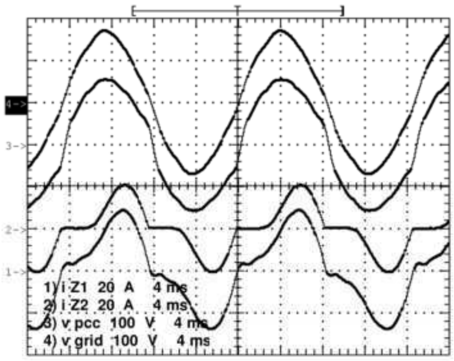

Fig. 8. Grid and PCC voltages and Z_1 and Z_2 line impedance currents - circuit without DGS.

TABLE V. GRID AND PCC VOLTAGE SPECTRA.

Harm.	**3°**	**5°**	**7°**	**9°**	**11°**	**13°**	**15°**
V_{grid} [%]	1.8	2.3	1.4	0.2	0.4	0.1	0.1
V_{PCC} [%]	7.4	4.5	2.6	1.9	1.7	0.7	0.3

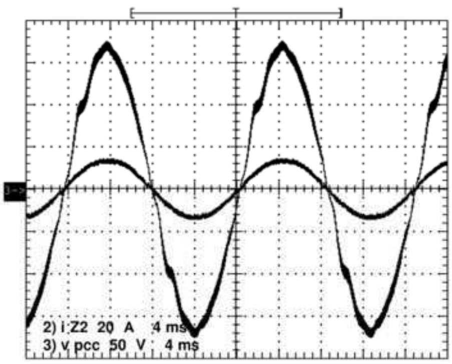

(a) SSC strategy without managing active power.

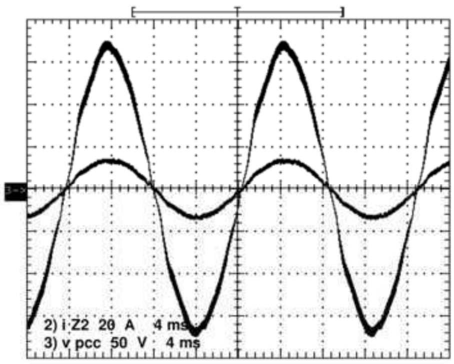

(b) RLS strategy without managing active power.

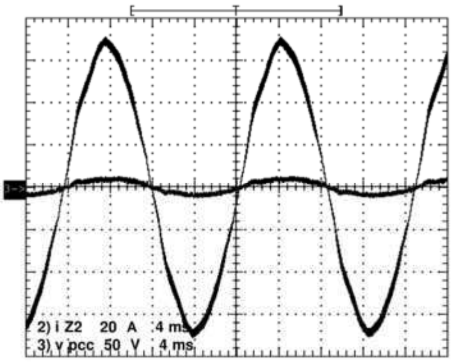

(c) RLS strategy and SCI strategy.

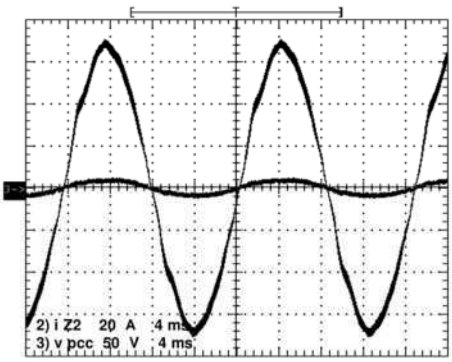

(d) RLS strategy and RCI strategy.

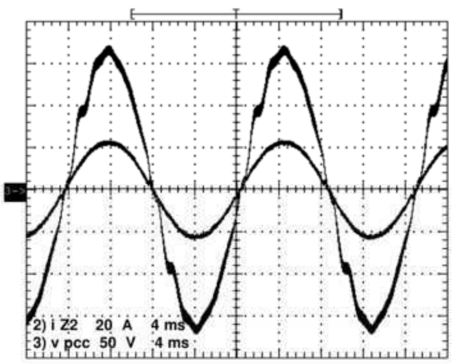

(e) SSC strategy and SCA strategy.

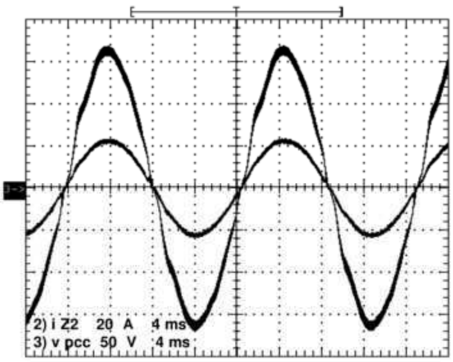

(f) SSC strategy and RCA strategy.

Fig. 9. Resistive current versus sinusoidal current for active power injection and current disturbances compensation.

Fig. 9.e and 9.f show the DGS compensating the load current disturbance by SSC strategy and absorbing about 800W of active power from the grid by SCA and RCA , respectively. In this case the R_{RES} has been connected to the DC link. From the PCC voltage point of view, it can be clearly observed that the active power absorption by RCA (Fig. 9.f) is better than the SCA (Fig. 9.e). All these results support the conclusions of section IV-A.

B. DGS selective compensation capability

Finally, Figs. 10 depict some experimental results of the DGS acting as an active compensator. The system used here is the same used for the simulations in section V-C, changing the Z_1 impedance, which is now the real grid line impedance with unknown value.

The local load has a power factor equal to 0.87 and current THD equal to 33%. Each Fig. (a-d) reports the PCC voltage {4} and current terms (inverter {1}, grid {2} and load {3}) using different current references.

Fig. 10.b shows that after compensation (RLS), the grid provides only part of the load active current demand and follows the PCC voltage waveform with high power factor (0.99) and low

total harmonic distortion (about 5.5%). Based on Table III, if we had used SSC compensation the inverter current should be practically sinusoidal, whereas the PCC voltage THD should be higher.

In this case, the inverter is set to inject about 50% of the load active power demand, as well as to provide non-active current compensation using (4). Note that 3.3% of the current THD comes from the distorted grid voltage, since RLS compensation strategy has been used. The sinusoidal active current injection (SCI), from Fig. 10.a, has about 2.5% of THD, which is due to the current controller.

In addition, Figs. 10.c and 10.d show the DGS injecting active power and simultaneously compensating only the reactive and void power, respectively.

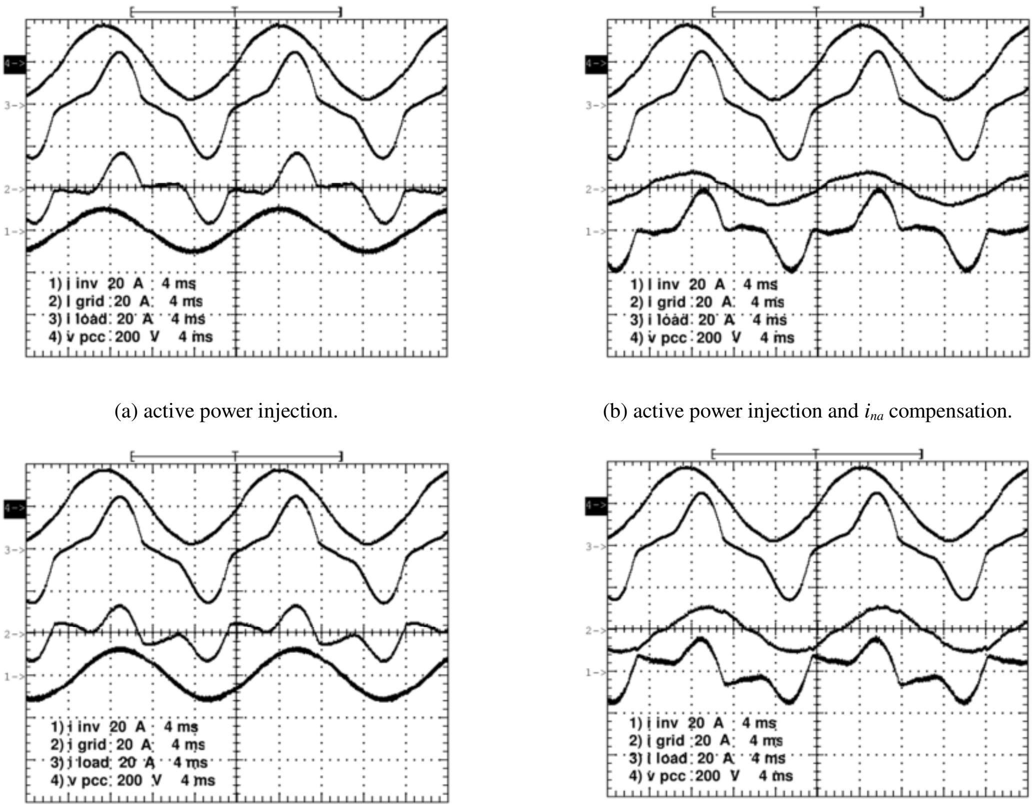

(a) active power injection.

(b) active power injection and i_{na} compensation.

(c) active power injection and i_r compensation.

(d) active power injection and i_v compensation.

Fig. 10. DGS providing active power from the RES and selective power quality compensation.

To analyze the selective compensation under load steps, Fig. 11 shows a raise of 40% on the load demand obtained by switching R_{ac} on. Fig. 11.a and Fig. 11.b show, respectively, the reactive and void selective compensation under the step disturbance, occurring in correspondence to the center of the visualized time interval. It can be observed that the system respond quite satisfactorily to external disturbances.

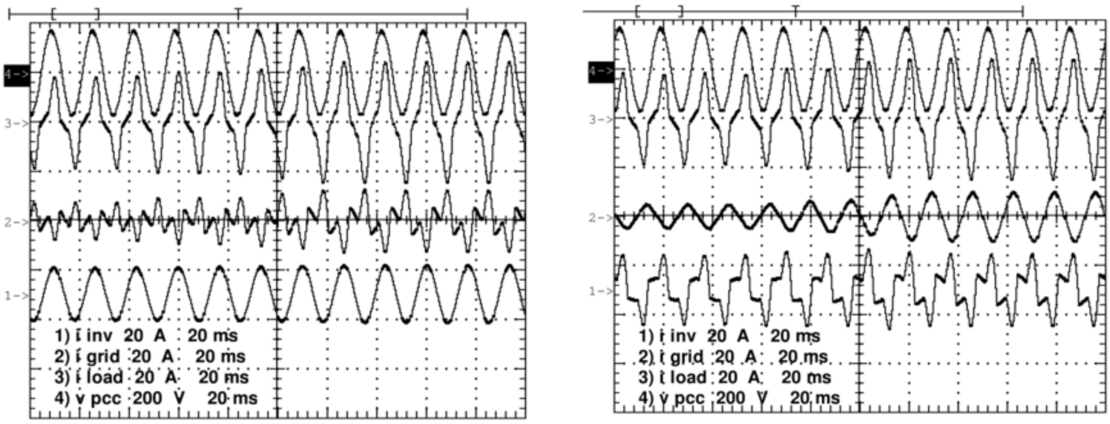

(a) active power injection and i_r compensation.

(b) active power injection and i_v compensation.

Fig. 11. DGS providing active power from the RES and selective compensation – dynamic response for load changing.

VII. CONCLUSIONS

This paper proposes a multi-task control strategy for distributed generation systems. The main functionalities are based on the CPT definitions, which gives flexibility to the system, especially when the instantaneous inverter capability is limited. As demonstrated, in addition to the active power injection, the proposed methodology allows voltage level regulation or selective load current disturbances mitigation. Note that the control strategies do not use any kind of reference-frame transformation and it can be applied without any additional consideration, even if the PCC voltage is non-sinusoidal.

It has also been shown that the best method to inject active power to the grid is using a sinusoidal current reference, as it avoids the amplification of possible resonances in the system. Conversely, in order to absorb active power from the grid, e.g. to charge a battery bank or to operate the inverter as a controlled rectifier, it is suggested to use a resistive current reference, to increase the damping effect on the PCC, minimizing possible resonant conditions.

ACKNOWLEDGMENT

The authors are grateful to FAPESP (proc. 2012/24309-8, 2012/14014-0 and 2013/08545-6), Fundunesp and CNPq (proc. 487471/2012-1 and 554960/2006-0) for the support provided to this research.

REFERENCES

[1] Mozina, C. J.: 'Impact of smart grids and green power generation on distribution systems', IEEE Trans. on Industry Applications, 2013, 49, (3), pp. 1079-1090.

[2] International Energy Outlook 2013: 'U.S. Energy Information Administration (EIA)', http://www.eia.gov/forecasts/aeo/, accessed April 2014.

[3] Carnieletto, R., Brandão, D. I., Farret, F. A., *et al.*: 'Smart grid initiative', IEEE Trans. on Industry Applications Magazine, 2011, 17, (5), pp. 27-35.

[4] Macken, K. J. P., Bollen, M. H. J., Belmans R. J. M.: 'Cost-effectiveness of distributed power quality compensation', IEEE Power Engineering Society General Meeting, 2003, pp. 1130-1135.

[5] Bidram, A., Davoudi, A., Lewis, F. L., Zhihua Qu: 'Secondary control of microgrids based on distributed cooperative control of multi-agent systems', IET Generation, Transmission & Distribution, 2013, 7, (8), pp. 822–831.

[6] Jinwei He, Yun Wei Li, Blaabjerg, F., *et al.*: 'Active harmonic filtering using current-controlled, grid-connected DG units with closed-loop power control', IEEE Trans. on Power Electronics, 2014, 29, (2), pp. 642-653.

[7] Jinwei He, Yun Wei Li, Munir, M. S.: 'A flexible harmonic control approach through voltage-controlled DG-grid interfacing converters', IEEE Trans. on Industrial Electronics, 2012, 59, (1), pp. 444-455.

[8] Wang, F., Duarte, J. L., Hendrix, M. A. M.: 'Design and analysis of active strategies for distributed generation inverters under unbalanced grid faults', IET Generation, Transmission & Distribution, 2010, 4, (8), pp. 905-916.

[9] Bojoi, R., Limongi, L. R., Roiu, D., *et al.*: 'Enhanced power quality control strategy for single-phase inverters in distributed generation systems', IEEE Trans. on Power Electronics, 2011, 26, (3), pp. 798-806.

[10] Maza-Ortega, J. M., Gómez-Expósito, A., Barragán-Villarejo, M., *et al.*: 'Voltage source converter-based topologies to further integrate renewable energy source in distributed systems', IET Renewable Power Generation, 2012, 6, (6), pp. 435-445.

[11] Ortjohann, E., *et al.*: 'A general architecture for modular smart inverters', IEEE International Symposium on Industrial Electronics, 2008, pp. 1525-1530.

[12] Kroposki, B., Pink, C., De Blasio, R., *et al*,: ‘Benefits of power electronic interfaces for distributed energy systems’, IEEE Trans. on Energy Conversion, 2010, 25, (3), pp.901-908.

[13] Tenti, P., Costabeber, A., Mattavelli, P., *et al*,: ‘Distribution loss minimization by token ring control of power electronic interfaces in residential microgrids’, IEEE Trans. on Industrial Electronics, 2012, 59, (10), pp. 3817-3826.

[14] Tenti, P., Costabeber, A., Mattavelli, P.: ‘Improving power quality and distribution efficiency in micro-grids by cooperative control of switching power interfaces’, International Power Electronics Conference, 2010, pp. 472-479.

[15] Tenti, P., Paredes, H. K. M., Mattavelli, P.: ‘Conservative power theory, a framework to approach control and accountability issues in smart microgrids’, IEEE Trans. on Power Electronics, 2011, 26, (3), pp. 664-673.

[16] Marafão, F. P., Brandão, D. I., Gonçalves F. A. S., Paredes, H. K. M.: ‘Decoupled reference generator for shunt active filter using the Conservative Power Theory’, Journal of Control, Automation and Electrical Systems, 2013, 24, pp. 522-534.

[17] Paredes, H K M.: ‘Conservative Power Theory: a new approach to cooperative control of power conditioners and considerations regarding to responsibility assignment’. PhD thesis, State University of Campinas, 2011, (in Portuguese).

[18] Zuniga, T. E. N., Pomilio J. A.: ‘Shunt active power filter synthesizing resistive load’, IEEE Trans. on Power Electronics, 2002, 16, (2), pp. 273-278.

[19] Marafão F. P., Deckmann, S. M., Pomilio, J. A., Machado, R. Q.: ‘Selective disturbance compensation and comparison of active filtering strategies’, IEEE International Conference on Harmonics and Quality of Power, 2002, pp. 484-489.

[20] Bollen, M. H. J., Sannino A.: ‘Voltage control with inverter-based distributed generation’ IEEE Trans. on Power Delivery, 2005, 20, (1), pp. 519-520.

[21] Brandão, D. I., Marafão, F. P., Simões, M. G., Pomilio, J. A.: ‘Considerations on the modeling and control scheme of grid connected inverter with voltage support capability’, Brazilian Power Electronics Conference, 2013.

[22] K. Ogata: ‘Modern control engineering’ (Prentice Hall, 2010, 5th edn).

[23] Mattavelli, P., Buso, S.: ‘Digital control in power electronics’ (Morgan & Claypoo, 2006, 1st edn).

[24] Chen, Z., Blaabjerg, F., Pedersen, J. K.: 'Harmonic resonance damping with a hybrid compensation system in power systems with dispersed generation' IEEE Power Electronics Specialist Conference, 2004, pp. 3070-3076.

[25] Fujita, H a., Akagi, H.: 'A practical approach to harmonic compensation in power systems-series connection of passive and active filters', IEEE Trans. on Industry Applications, 1991, 27, (6), pp. 1020-1025.

[26] Wada, K., Fujita, H., Akagi, H.: 'Considerations of a shunt active filter based on voltage detection for installation on a long distribution feeder', IEEE Trans. on Industry Applications, 2002, 38, (4), pp. 1123-1130.

[27] Canesin, C. A., Brito, M. A. G., Sampaio, L. P., *et al.*: 'Evaluation of main MPPT techniques for photovoltaic applications', IEEE Trans. on Industrial Electronics, 2013, 60, (3), pp. 1156-1167, 2013.

[28] Pomilio, J. A., Deckmann, S. M.: 'Characterization and compensation of harmonic and reactive power of residential and commercial loads', IEEE Trans. on Power Delivery, 2007, 22, (2), pp. 1049-1055.